Structure, Vol. 11, 1569–1581, December, 2003, ©2003 Elsevier Science Ltd. All rights reserved. DOI 10.1016/j.str.2003.10.016

The Yeast YPD1/SLN1 Complex: Insights into Molecular Recognition in Two-Component Signaling Systems

Qingping Xu,[1,2] Stace W. Porter,[1] and Ann H. West[1,*]
[1]Department of Chemistry and Biochemistry
University of Oklahoma
620 Parrington Oval
Norman, Oklahoma 73019

Summary

In *Saccharomyces cerevisiae*, a branched multistep phosphorelay signaling pathway regulates cellular adaptation to hyperosmotic stress. YPD1 functions as a histidine-phosphorylated protein intermediate required for phosphoryl group transfer from a membrane-bound sensor histidine kinase (SLN1) to two distinct response regulator proteins (SSK1 and SKN7). These four proteins are evolutionarily related to the well-characterized "two-component" regulatory proteins from bacteria. Although structural information is available for many two-component signaling proteins, there are very few examples of complexes between interacting phosphorelay partners. Here we report the first crystal structure of a prototypical monomeric histidine-containing phosphotransfer (HPt) protein YPD1 in complex with its upstream phosphodonor, the response regulator domain associated with SLN1.

Introduction

Two-component signaling pathways typically involve histidine-to-aspartate phosphoryl transfer between a membrane-bound sensor histidine protein kinase and a cytoplasmic response regulator protein. Two-component systems regulate a wide variety of important cellular processes, such as cell motility, cell cycle control, development, antibiotic resistance, microbial and fungal pathogenesis, as well as responses to hormonal stimuli and environmental stress in bacteria, archaea, amoebae, fungi, and plants (Hoch and Silhavy, 1995; Saito, 2001; Stock et al., 2000; Urao et al., 2000; West and Stock, 2001). In some cases, an additional signaling module referred to as a histidine-containing phosphotransfer (HPt) protein or domain is employed and the simple two-component system is thus expanded into a more complex multistep phosphorelay system (West and Stock, 2001).

In *Saccharomyces cerevisiae*, the HPt protein YPD1 is required for phosphoryl group transfer from the membrane-bound hybrid sensor kinase (SLN1) to two downstream response regulators, SSK1 and SKN7, both of which are involved in environmental stress responses (Brown et al., 1994; Ketela et al., 1998; Li et al., 1998; Posas et al., 1996). The interaction of YPD1 with the response regulator domains associated with the SLN1, SSK1, and SKN7 proteins (referred to as the R1, R2, and R3 domains, respectively) suggests that YPD1 is somewhat promiscuous and may have characteristic molecular surface features that allow it to bind several different response regulator domains.

The previously determined structure of the 19.2 kDa YPD1 protein revealed an all-helical tertiary fold with a four helix bundle core (Xu and West, 1999; Song et al., 1999). The phosphorylatable histidine (His64) is solvent exposed and protrudes out from the surface of the helical bundle. We have used complementary approaches to investigate the structural basis of interaction between YPD1 and response regulator domains. One approach employs alanine-scanning mutagenesis coupled to an in vivo yeast two-hybrid screen in order to identify YPD1 residues that are required for protein-protein interactions. In previous work, we focused on the interaction between YPD1 and SSK1-R2, whereby a potential response regulator docking site was identified on one face of YPD1 located between the site of phosphorylation (His64) and the αA helix (Porter et al., 2003). The SSK1-R2 response regulator binding surface on YPD1 is composed of a large hydrophobic patch (approximately 690 Å^2) surrounded by polar and charged residues. Due to the sequence conservation of residues within this region, we postulated that this hydrophobic patch is involved in general binding of HPt domains to response regulator proteins (Porter et al., 2003).

A more direct approach is to attempt to cocrystallize phosphorelay partners in order to obtain information regarding protein-protein interactions at the atomic level. However, structures of complexes between two-component phosphorelay signaling proteins have been difficult to study due, in part, to the transient nature of the interaction, and the chemical lability of phosphohistidinyl and phospho-aspartyl linkages. Here we report X-ray crystallographic analysis of a complex between YPD1 and the SLN1 response regulator domain (YPD1/SLN1-R1). The SLN1-R1 structure is only the second structure determined of a eukaryotic response regulator domain and, as expected, shows a very high degree of structure conservation in comparison to the plant ETR1 structure (Müller-Dieckmann et al., 1999) and bacterial response regulator domains. The structure of the YPD1/SLN1-R1 complex allows for the first time a detailed analysis of the mode of interaction between a prototypical monomeric HPt protein and its cognate response regulator domain. Furthermore, because of the high degree of structural homology among HPt proteins and within the response regulator superfamily, the YPD1/SLN1-R1 complex can serve as a good model for studies of other HPt protein-response regulator complexes.

Results and Discussion

Overall Structure of the Complex

Two crystal forms of the YPD1/SLN1-R1 complex were obtained under similar crystallization conditions (Choo-

*Correspondence: awest@chemdept.chem.ou.edu
[2]Present address: Stanford Linear Accelerator Center, 2575 Sand Hill Road, Mail Stop 99, Menlo Park, California 94025.

Table 1. Data Collection and Refinement Statistics

	Crystal Form I	Crystal Form II
Data collection		
Space group	$P3_2$	$P2_12_12_1$
Cell dimensions (Å)	a = b = 91.3, c = 200.35	a = 51.73, b = 74.25, c = 98.80
Resolution (Å)	30–2.1	30–2.3
Mean I/σ (I)	30.7(6.4)[d]	19.0 (6.5)
Number of observations	539,449	84,027
Unique reflections	104,137	17,319
Completeness (%)	95.6 (72.1)	98.3 (94.5)
R_{merge}[a]	0.053 (0.186)	0.05 (0.239)
Refinement		
Resolution range (Å)	30–2.1	30–2.3
R factor[b]/R_{free}[c]	23.6 (25.8)	21.4 (26.6)
Average B factor (Å^2)	29.43	38.71
Complexes per *asu*	6	1
No. of protein atoms	13,332	2,292
No. of solvent molecules	225 (18 SO_4^{2-} + 207 H_2O)	55 (1 SO_4^{2-} + 54 H_2O)
Rms deviation		
Bond length (Å)	0.020	0.012
Bond angle (°)	1.73	1.40
Ramachandran plot, % residues in:		
Most favored region	94.1	90.9
Additionally allowed region	5.5	7.9
Generously allowed region	0.0	0.8
Disallowed region	0.4	0.4

[a] $R_{merge} = \Sigma|I - \langle I\rangle|/\Sigma|I|$, where I is the intensity measurement for a given reflection, and $\langle I\rangle$ is the average intensity for multiple measurements of this reflection.

[b] R factor $= \Sigma||F_{obs}| - |F_{calc}||/\Sigma|F_{obs}|$, where $|F_{obs}|$ and $|F_{calc}|$ are observed and calculated structure factor amplitudes, respectively.

[c] R_{free} was calculated using 5% and 10% of the diffraction data that were selected randomly and not used throughout the refinement for crystal form I and II, respectively.

[d] Values in parentheses correspond to the highest resolution shell.

back and West, 2003). The structures of the complex were determined by molecular replacement using the YPD1 structure (Xu and West, 1999) (PDB code: 1QSP) as a search model. The final models were refined to a resolution of 2.1 and 2.3 Å with corresponding R factors of 23.6% (R_{free} = 25.8%) and 21.4% (R_{free} = 26.6%) for the structures obtained in space groups $P3_2$ and $P2_12_12_1$, respectively (Table 1). There are six 1:1 YPD1/SLN1-R1 complexes per asymmetric unit in the $P3_2$ crystal form that are related to each other (average rms deviation of ~0.3 Å between C_α atoms among the six complexes) by 2-fold and 3-fold noncrystallographic symmetry. There is only one 1:1 complex in the asymmetric unit for the $P2_12_12_1$ crystal form.

Overall, the structures of the individual proteins determined in the two different space groups do not differ significantly from one another. The rms deviation is ~0.62 Å for 124 aligned C_α atoms between SLN1-R1 domains and ~0.61 Å for 155 aligned C_α atoms between YPD1 molecules in the two crystal forms. Furthermore, the YPD1 structure in the complex does not differ significantly from the YPD1 structure determined by itself (rms deviation of 1.12 and 0.56 Å for the $P2_12_12_1$ and $P3_2$ complex, respectively, as compared to the 1QSP model (Xu and West, 1999). The ribbon structure of the YPD1/SLN1-R1 complex in $P2_12_12_1$ is shown in Figure 1A. YPD1 is positioned relative to SLN1-R1 such that the four helix bundle of YPD1 is almost perpendicular to the central β sheet of SLN1-R1 (Figure 1). The phosphorylatable histidine, His64, of YPD1 is in close proximity to the SLN1-R1 active site. However, the main difference between the two crystal complexes is a rigid body displacement of YPD1 with respect to SLN1-R1 (corresponding to about 6.1 Å rms deviation between YPD1 molecules). By superimposing the SLN1-R1 domains from the two complex structures, the difference in the location and orientation of YPD1 as compared to SLN1-R1 in the two crystal forms is illustrated in Figure 1B. Residues from the αA, αB, and αC helices encompassing the site of phosphorylation (His64) of YPD1 form a complementary surface that provides a docking site for SLN1-R1, which binds YPD1 primarily through its α1 helix and four out of the five loops surrounding the active site (Figures 1A and 1C).

The SLN1 response regulator domain is located at the C terminus of the SLN1 hybrid sensor histidine kinase and consists of 136 residues (residues 1084–1220 in the primary sequence). The SLN1-R1 domain shares both sequence (29% identity/53% homology) and functional homology with the bacterial response regulator CheY. The crystal structure of SLN1-R1 revealed in this study has the same overall tertiary fold $(\beta\alpha)_5$ as CheY and about a dozen other bacterial response regulator domains for which structures have been determined (reviewed in Robinson et al., 2000; Stock et al., 2000; West and Stock, 2001). The SLN1-R1 domain has an rms deviation of only 1.27 Å for 117 aligned C_α atoms when superimposed with the structure of *E. coli* CheY (Volz and Matsumura, 1991). The main difference is in the length of helix α5, which is shorter by about 5 residues in SLN1-R1 and shows larger backbone differences as compared to CheY. The C terminus of SLN1-R1 forms an extended

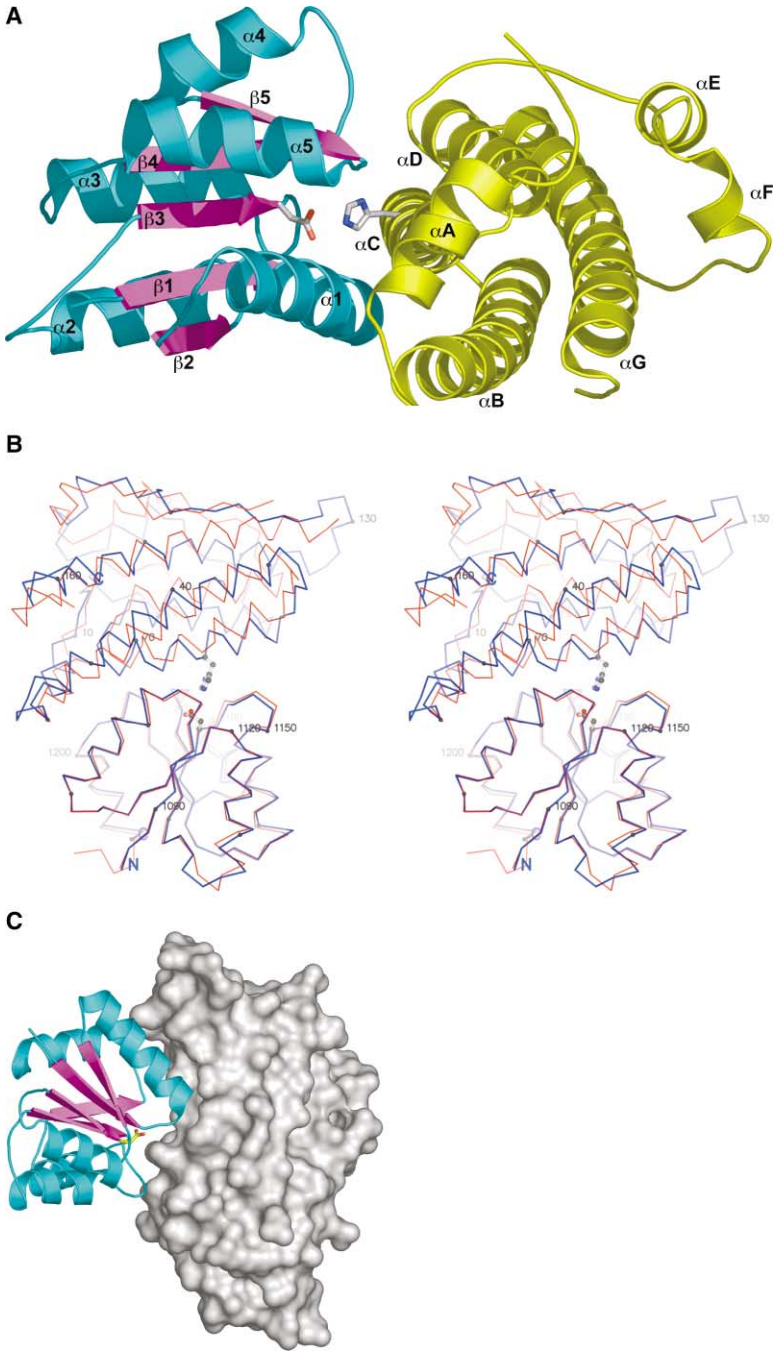

Figure 1. Structure of the YPD1/SLN1-R1 Complex

(A) Ribbon representation illustrates the relative positioning of YPD1 (yellow) with respect to the SLN1 response regulator domain R1 (cyan and magenta) as seen in the crystalline $P2_12_12_1$ complex. The side chains for His64 of YPD1 and Asp1144 of SLN1-R1 that are involved in phosphotransfer are shown in stick model.

(B) Stereoview overlay of the Cα trace of YPD1/SLN1-R1 complex structures obtained in the two crystal forms. The SLN1-R1 domains (bottom) from the two crystal forms were superimposed onto each other to illustrate the slightly different binding modes of YPD1 (top) observed in the $P2_12_12_1$ (shown in blue with residue numbers) versus $P3_2$ (shown in red) crystal forms.

(C) A view approximately 90° away from Figure 1B showing the molecular surface of YPD1 (gray) and a ribbon diagram of SLN1-R1 (cyan and magenta), which highlights the surface complementarity at the binding interface in the $P2_12_12_1$ complex.

loop containing residues 1211–1220 that are disordered. Based on structural comparisons between SLN1-R1 and other response regulator domains, the central parallel β sheet and backbone conformations in and around the active site are highly conserved, whereas the regions on the opposite face of the molecule, such as the α→β loops, exhibit greater sequence and length variability. For example, the loop between α2 and β3 in SLN1-R1 is about 5 residues longer than the corresponding loop of CheY. Among the β→α loops that form the active site, the backbone of loops β1-α1, β2-α2, and β3-α3 are more conserved (i.e., they have lower rms deviation in comparison to CheY) than the β4-α4 and β5-α5 loops.

Interestingly, the SLN1-R1 structure exhibits greater sequence and structure similarity to bacterial CheY (as cited above) than it does to the plant ETR1 response regulator domain (26% sequence identity/48% homology; rms deviation of 1.34 Å for 105 aligned Cα atoms). Overall, the SLN1-R1 structure in comparison to other bacterial response regulator domains (Baikalov et al., 1996; Birck et al., 1999; Djordjevic et al., 1998; Madhusudan et al., 1996; Stock et al., 1993; Volkman et al., 1995) and ETR1 from *Arabidopsis* (Müller-Dieckmann et al., 1999) indicates evolutionary conservation of the response regulator three-dimensional structure and function.

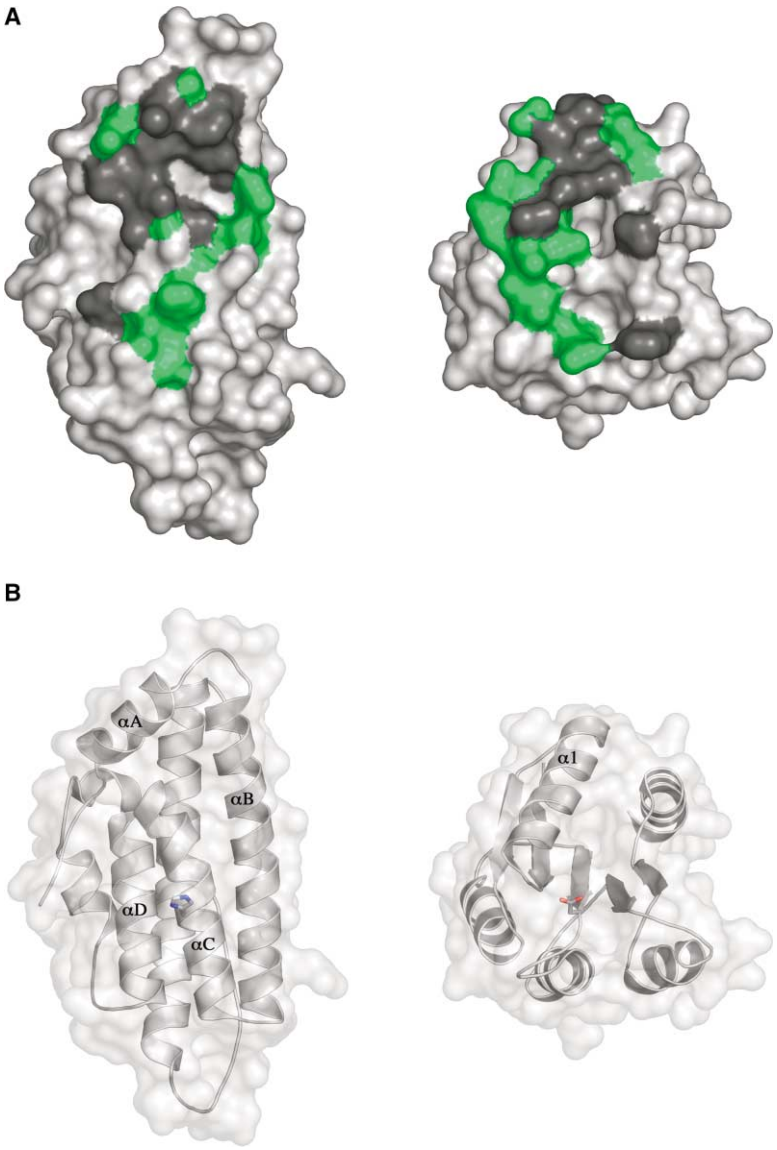

Figure 2. YPD1/ SLN1-R1 Interaction Surface

(A) The binding surfaces are highlighted with respect to hydrophobic (dark gray) versus polar (green) character on YPD1 (left panel) and SLN1-R1 (right panel) as observed in the $P2_12_12_1$ crystal complex. The two molecules in the complex were rotated approximately 90° (in opposite directions) and translated apart to face the viewer.

(B) The same view of YPD1 and SLN1-R1 as in Figure 2A but with a transparent molecular surface and an underlying ribbon representation to illustrate the location of important secondary structure elements (labeled) discussed in the text. Side chains for the active site residues, His64 in YPD1 and Asp1144 in SLN1-R1, are shown in stick model.

Analysis of the Binding Interface

The YPD1/SLN1-R1 binding interface features a buried patch of hydrophobic area flanked by hydrophilic interactions (Figure 2A). The buried surface area contributed by YPD1 in the $P2_12_12_1$ complex is 953 Å^2 (11.5% of the total surface area of YPD1), characteristic of weakly interacting proteins (Nooren and Thornton, 2003). Residues from YPD1 that make contact with SLN1-R1 come from helices αA, αB, αC, and αD (Figure 2B; Table 2). The surface-exposed face of helix A in YPD1, which contains several hydrophobic residues (Ile13, Ile17, and Met20), makes extensive contact with the SLN1-R1 domain, and we predict that this is important in mediating complex formation. The binding surface on SLN1-R1 consists of residues located along the α1 helix and several loops surrounding the active site, specifically β1-α1, β3-α3, β4-α4, and β4-α4 (Figure 2B; Table 2). Surface residues from the α1 helix of SLN1-R1 are mainly hydrophobic in nature and contribute a large part of the binding surface forming interactions with αA, αB, and αC of YPD1 (Figure 2). The α1 helix of SLN1-R1 is oriented nearly parallel to helix C of YPD1 (ω = 26.6°, defined in PROMOTIF [Hutchinson and Thornton, 1996]) and is nestled between the αB and αC helices of YPD1 (Figure 3A). The N-terminal portion of the α5 helix and the conserved β5-α5 loop of SLN1-R1 also make hydrophobic contacts with the N-terminal portion of helix αA in YPD1. The remaining loop regions that form the active site of SLN1-R1, with the exception of β2-α2 loop, also constitute a large portion of the binding interface. These loops mainly make contact to YPD1 near the perimeter of the hydrophobic docking surface of YPD1.

Due to the difference in position of YPD1 relative to SLN1-R1, the overall interface area contributed by YPD1 is less extensive in the $P3_2$ complex (678 Å^2) than the $P2_12_12_1$ model (Figure 3B). Analysis of the positioning of α1 of SLN1-R1 relative to αC of YPD1 (ω = 16.4°) indicates the molecules are rotated approximately 10° relative to one another in the two crystal forms. One consequence of this rotation is that the β4-α4 loop from

Table 2. YPD1/SLN1-R1 Intermolecular Contacts

YPD1 Residue	Location	SLN1-R1 Residue(s)	Location
$P2_12_12_1$ Complex			
Hydrophobic interactions[a]			
Ile13	αA	Pro1196	β5-α5 loop
Ile17	αA	Val1102	α1
Met20	αA	Arg1105, Met1106, Leu1109	α1
Phe27	αB	Arg1105	α1
Leu31	αB	Val1102	α1
Ser69	αC	Val1098	α1
Ala71	αC	Pro1196	β5-α5 loop
Ala72	αC	Pro1196, Val1102	β5-α5 loop, α1
Glu83	αD	Phe1175	β4-α4 loop
Hydrogen bond interactions[b]			
Glu16 Oε1	αA	Arg1199 N	α5
Met20 O	αA	Arg1105 Nη2	α1
Gln34 Nε2	αB	Glu1101 Oε2	α1
Gln34 Oε1	αB	His1097 Nδ1	α1
Gln38 Nε2	αB	Asn1096 Oδ1	β1-α1 loop
Gln38 Oε1	αB	Asn1096 Nδ2	β1-α1 loop
Asp60 Oδ1	αC	Gln1146 Nε2	β3-α3 loop
His64 Nε2	αC	Asp1095 Oδ2	β1-α1 loop
Phe65 O	αC	Asn1096 Nδ2	β1-α1 loop
Gly68 O	αC	Asn1099 Nδ2	α1
Gln86 Oε1	αD	Gln1146 Nε2	β3-α3 loop
Arg90 Nη2	αD	Gln1146 Oε1	β3-α3 loop
$P3_2$ Complex			
Hydrophobic interactions[a]			
Ile13	αA	Pro1196	β5-α5 loop
Ile17	αA	Val1102	α1
Met20	αA	Arg1105, Met1106, Leu1109, Arg1199	α1, α5
Phe27	αB	Arg1105	α1
Leu31	αB	Glu1101, Val1102	α1
Gln34	αB	Val1098	α1
Ser69	αC	Val1098	α1
Hydrogen bond interactions[b]			
Glu16 Oε1	αA	Arg1199 N	α5
Ser19 Oγ	αA	Arg1199 Nη2	α5
Met20 O	αA	Arg1105 Nη1, Arg1105 Nε	α1
Gln38 Nε2	αB	Asn1096 Oδ1	β1-α1 loop
Gln38 Oε1	αB	Asn1096 Nδ2	β1-α1 loop
His64 Nε2	αC	Asp1095 Oδ2	β1-α1 loop
Phe65 O	αC	Asn1096 Nδ2	β1-α1 loop
Gly68 O	αC	Asn1099 Nδ2	α1

[a] Identified using the programs LigPlot (Wallace et al., 1995), SURFNET (Laskowski, 1991), and by visual inspection.
[b] Identified using the HBPLUS algorithm as implemented in LigPlot (Wallace et al., 1995) with donor-acceptance cutoff distance of ≤3.2 Å.

SLN1-R1 loses contact with helix αD of YPD1 (Figure 3B). This results in a significant reduction in buried surface area for the $P3_2$ complex (290 Å^2 less) relative to the $P2_12_12_1$ complex. New contacts are made between the αA helix of YPD1 and α5 of SLN1-R1, which contribute to the buried surface area of the $P3_2$ complex (Table 2).

In both crystal forms, the hydrophobic contacts between the α1 of SLN1-R1 and YPD1 are maintained (Figure 3; Table 2). However, the position of this helix is different in the two crystal forms. In the $P2_12_12_1$ model, the relative difference in positioning of the SLN1-R1 domain with respect to YPD1, results in the α1 helix from SLN1-R1 being rotated slightly away from helix αB toward helix αC of YPD1. The β4-α4 loop of SLN1-R1 is not in contact with YPD1 in the $P3_2$ model, but does form contacts with helix αD (around Gln86) of YPD1 in the $P2_12_12_1$ model. In the $P3_2$ model, the α1 helix of SLN1-R1 is nestled between the αB and αC helices of YPD1 in an almost parallel fashion.

Another important difference between the two crystal forms is the distance between His64 of YPD1 to the active site of SLN1-R1. In the $P2_12_12_1$ complex, His64 of YPD1 is closer to the acidic active site pocket of SLN1-R1 and is within a more reasonable distance to Asp1144 of SLN1-R1 for phosphoryl transfer. The Nε2 atom of His64 is 3.91 and 5.78 Å away from the Oδ2 atom of Asp1144 in the $P2_12_12_1$ and $P3_2$ crystal complexes, respectively. Additionally, the two active sites become buried in the $P2_12_12_1$ complex, whereas the active site area in the $P3_2$ model is more accessible to bulk solvent.

In the $P2_12_12_1$ complex, there are only a few water-mediated contacts at the interface, whereas in the $P3_2$ complex, none were observed. It is interesting to note, however, that the ratio of polar to nonpolar residues at

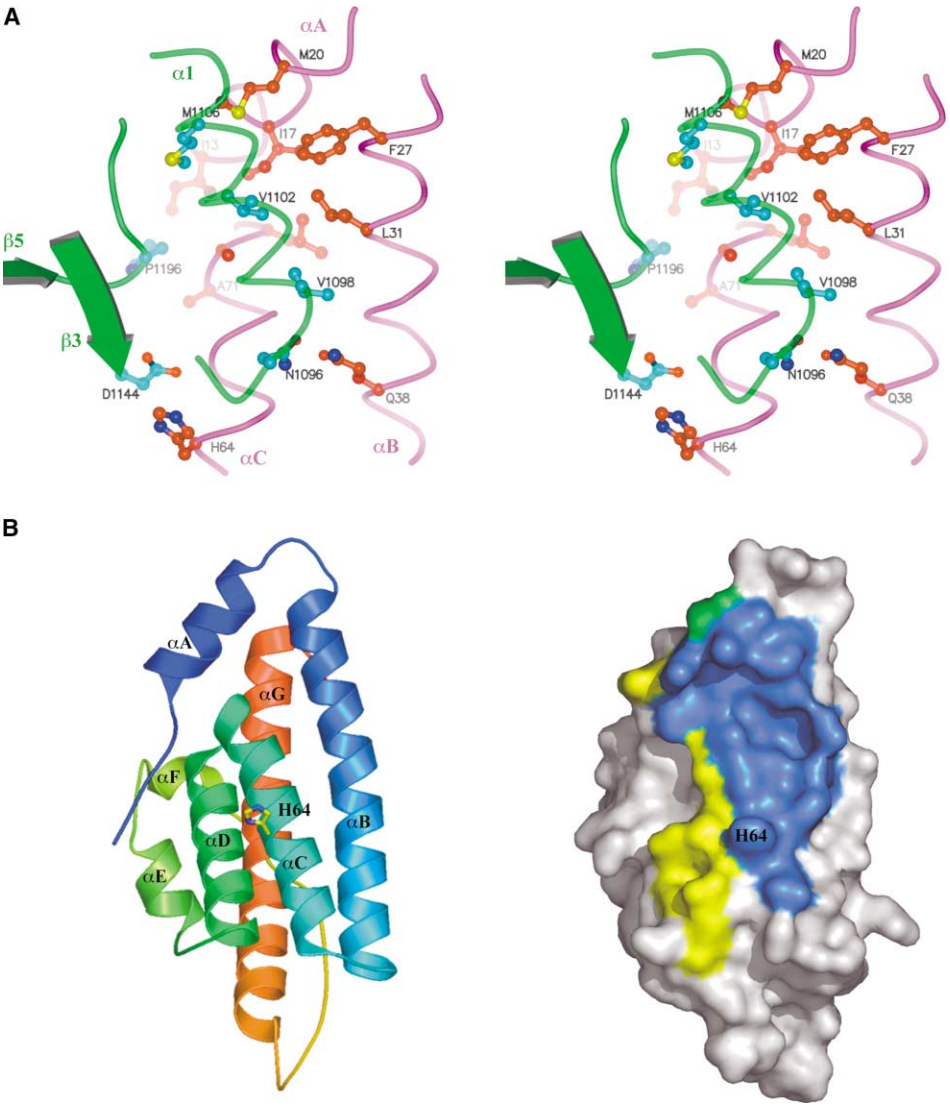

Figure 3. Interactions between SLN1-R1 and YPD1

(A) Stereoview illustrates the hydrophobic contacts at the binding interface involving residues from the αA, αB, and αC helices in YPD1 (magenta) and residues from the α1 helix in SLN1-R1 (green).

(B) A ribbon diagram (on the left) illustrates the location of secondary structure elements corresponding to the same orientation shown in the molecular surface view of YPD1 (on the right). The common interface shared by both crystal complexes is colored blue and the additional binding surface specific to the $P2_12_12_1$ or $P3_2$ crystal complex is colored yellow and green, respectively, in the molecular surface representation.

the interface of the two crystal forms is very similar (both interfaces are ~65% nonpolar). For both complexes, a relatively low gap index (Jones et al., 2000; Nooren and Thornton, 2003) was calculated, which indicates a very high degree of surface complementarity.

Although one cannot rule out the effects of crystal packing completely, the fact that the two models were obtained under similar conditions suggests that there are at least two possible modes of binding between SLN1-R1 and YPD1. A common hydrophobic binding site is observed in both crystal forms. Since YPD1 and SLN1-R1 are associated in the $P3_2$ crystal form through a smaller binding interface, in what might be a lower affinity complex, it is plausible that the complex in the $P3_2$ crystal form may represent an initial stable complex between YPD1 and SLN1-R1 with the common hydrophobic patch serving as an initial recognition site. Alternatively, the $P3_2$ crystal form may be the result of a low-affinity complex formed after phosphotransfer has occurred but just prior to dissociation of the two molecules.

The binding interface of the $P2_12_12_1$ model correlates very well with the surface identified by yeast two-hybrid analysis of the interaction between YPD1 and the downstream response regulator SSK1-R2 (Porter et al., 2003). Most of the mutations on the surface of YPD1 that disrupt complex formation with SSK1-R2 (e.g., Ile13, Met20, Phe27, Leu31, and Phe65) are clustered around the conserved hydrophobic interfaces observed in both YPD1/SLN1-R1 crystal complexes (Figure 2A). Further-

more, the yeast two-hybrid data obtained with YPD1 and SSK1-R2 indicated several polar residues located near the hydrophobic binding patch (e.g., Glu16, Asp21, Gln38, Asp60, Gly68, Ser69, and Gln76) are also important for protein-protein interaction. Although structural information at the level of atomic resolution is not yet available for the SSK1-R2 domain (or any complex), it was very interesting to note that a large majority of the YPD1 residues involved in interaction with SLN1-R1 (Table 2) were also found to be important for interaction with SSK1-R2 (Porter et al., 2003). All things considered, we believe that the conformation of the YPD1/SLN1-R1 complex obtained in the $P2_12_12_1$ crystal form is more likely than the $P3_2$ complex to represent a productive complex in which His64 of YPD1 and Asp1144 of SLN1-R1 are properly aligned and within reasonable distance to each other for phosphotransfer to occur.

Conservation of HPt Protein/Response Regulator Protein Interactions

It has been well documented that the *E. coli* ArcB^c (Kato et al., 1997) and CheA-P1 (Mourey et al., 2001; Zhou and Dahlquist, 1997) HPt domains share very similar chemical and structural features in comparison to YPD1 (Xu and West, 1999; Song et al., 1999). From this study, it became apparent that the CheA-P1 and ArcB^c domains have a similar arrangement and conservation of surface-exposed hydrophobic residues as compared to YPD1 (Figures 4A and 4B, respectively), with the exception of residues from the αA helix that are missing in the CheA-P1 domain. Since many of these residues in YPD1 are directly involved in response regulator binding, we suggest that other HPt proteins also bind to their cognate response regulator in a similar manner involving exposed hydrophobic residues from regions of the protein corresponding to the αA, αB, and αC helices in YPD1.

Despite the common hydrophobic patch, there are significant differences in how additional surfaces are involved in HPt protein/response regulator binding. For example, with the CheA/CheY system, CheA does not have an equivalent αA helix observed in YPD1, hence the binding interface between CheA-P1 and CheY is expected to be less extensive. This may explain why the CheA-P2 domain is required for binding CheY because it contributes approximately another 600 Å^2 of binding surface (McEvoy et al., 1998; Welch et al., 1998).

Since YPD1 exhibits a high degree of structural homology to the CheA-P1 domain (Mourey et al., 2001), and likewise, SLN1-R1 is structurally and functionally related to CheY, the YPD1/SLN1-R1 complex can serve as a reasonably good model for examining possible interactions between the CheA P1 domain and the response regulator CheY. Thus, using the structures of Mg^{2+}-bound CheY (Stock et al., 1993) and the CheY/CheA-P2 complex (Welch et al., 1998), a reasonable ternary complex between CheY and the P1 and P2 domains of CheA was modeled based on the YPD1/SLN1-R1 complex (Figure 4D). This analysis identifies two potentially important areas of hydrophobic interactions involving the CheA P1 domain: the hydrophobic residues at the N-terminal portion of αA (equivalent to αB of YPD1) and a hydrophobic cluster around Phe59 (total estimated binding interface is ~470 Å^2). In the modeled complex, the distance between the C terminus of the CheA-P1 domain and N terminus of the P2 domain can easily be accommodated by the missing 28 residue interdomain linker region.

The YPD1/SLN1-R1 complexes in the two crystal forms share a common hydrophobic binding interface. The exposed hydrophobic residues on the surface of SLN1-R1 that form part of the binding interface are Val1098, Val1102, Met1106, and Leu1109 from helix α1 and Pro1196 from the β5-α5 loop (Figure 3A; Table 2). Interestingly, the corresponding α1 helix and β5-α5 loop from the *Bacillus subtilis* Spo0F response regulator are also involved in forming similar contacts to Spo0B, a dimeric HPt protein (Figure 5) (Zapf et al., 2000). Spo0B binds Spo0F through a more extensive interface (buried surface area of ~1200 Å^2) than the YPD1/SLN1-R1 complex (Zapf et al., 2000). The primary difference in mode of binding is that the response regulator Spo0F binds to Spo0B such that contacts are made to a flanking C-terminal α/β domain as well as an elongated four helix bundle. Based on the overall structure of Spo0B and its striking similarities to the histidine-containing dimerization domain of histidine kinases, like EnvZ (Tomomori et al., 1999), we would argue that the Spo0B/Spo0F complex is characteristic of histidine kinase-response regulator interactions, whereas the YPD1/SLN1-R1 complex is representative of HPt protein-response regulator interactions.

Despite the fact that there is virtually no sequence homology between Spo0B and YPD1, the overall arrangement between the phosphotransfer protein and the response regulator, as well as the secondary structure elements involved in binding, are similar in the YPD1/SLN1-R1 and Spo0B/Spo0F complexes. However, when the two complexes were superimposed with respect to the response regulator domains, there was very poor structural alignment between YPD1 and Spo0B, as illustrated in Figure 4C. Like the CheA-P1 domain, Spo0B does not contain a corresponding αA helix as in YPD1 (Kato et al., 1997). Instead, the two antiparallel helix motifs (one from each monomer) in Spo0B that are involved in binding Spo0F are longer by about 12 Å than the helical bundles observed in monomeric HPt proteins (Figure 5). The extended helices occupy the same location as the αA helix of YPD1. Moreover, key residues on the surface of Spo0B, which are involved in binding Spo0F map to these extended helices (Zapf et al., 2000). Although there is conservation of functional structural motifs (i.e., antiparallel helices forming four helix bundles) between YPD1 and Spo0B, the lack of sequence homology and the difference in overall structure suggest that these two HPt proteins may have evolved from different ancestors.

The residues contributing to the hydrophobic patch on the interacting surface of SLN1-R1 (particularly those from α1 and the β5-α5 loop) are highly conserved within the family of eukaryotic response regulator domains (S.W.P. and A.H.W., unpublished data) and numerous bacterial response regulators including CheY and Spo0F (Zapf et al., 2000; Hoch and Varughese, 2001). The presence of conserved hydrophobic surfaces on both response regulators and HPt proteins suggests that the

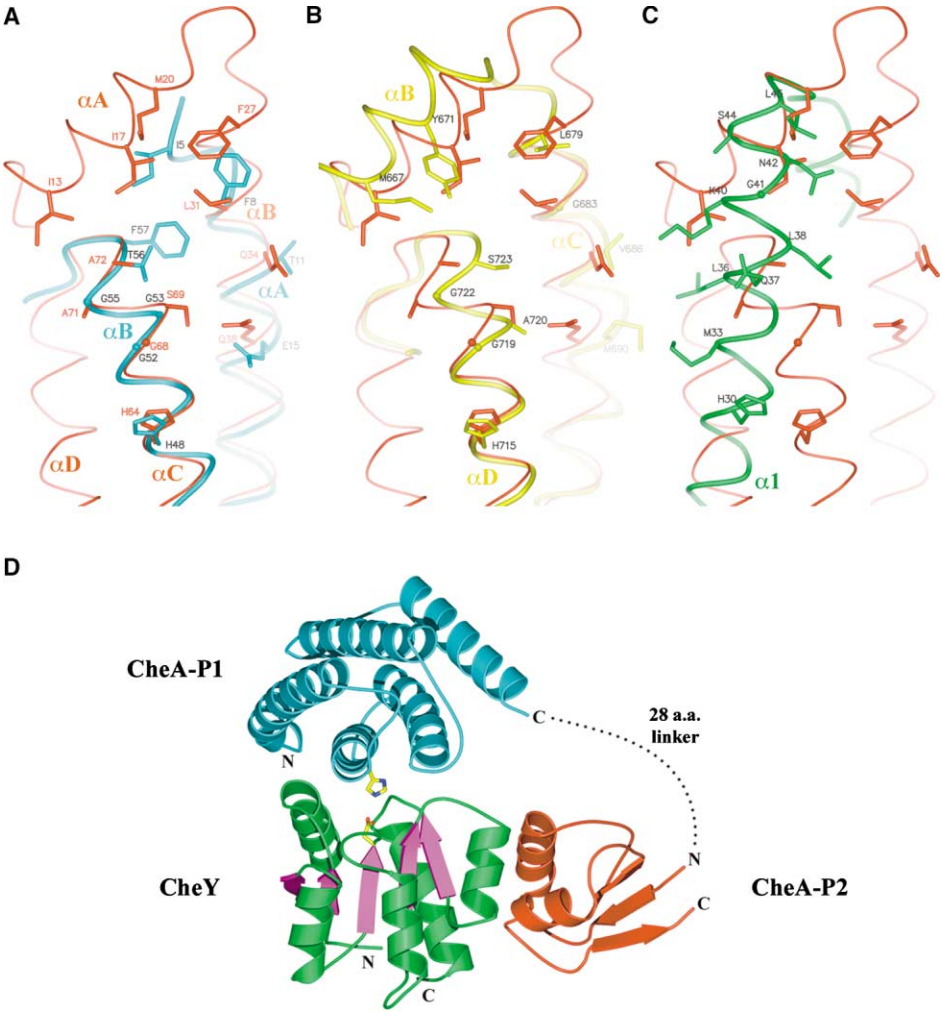

Figure 4. Comparison of HPt Protein and Response Regulator Protein Interactions

(A and B) Overlay of the YPD1 (red) hydrophobic response regulator docking site with the CheA-P1 domain (cyan) (A) and the ArcB^c HPt domain (gold) (B) shows that the hydrophobic patch on YPD1 is conserved in other HPt domains.

(C) Superposition of the response regulator proteins from the YPD1/SLN1-R1 complex and the Spo0B/Spo0F complex shows poor structural alignment in the region of the αA-αD helices from YPD1 (red) and the α1-α2 helices from Spo0B (green).

(D) Modeled ternary complex between CheY (green/magenta) and the CheA-P1 (cyan) and P2 (red) domains. The active site residues for CheA-P1 (His48) and CheY (Asp57) are shown in stick model. The dashed line represents a 28 residue linker region joining the CheA-P1 and P2 domains for which structural information is unknown.

interaction mode observed in the YPD1/SLN1-R1 complex represents a general scheme of intermolecular interaction employed in two-component signaling systems. For example, all structurally known HPt proteins and histidine kinases contain a conserved four helix bundle motif with similarly located histidine phosphorylation sites (Kato et al., 1997; Mourey et al., 2001; Song et al., 1999; Tomomori et al., 1999; Varughese et al., 1998; Xu and West, 1999; Zhou and Dahlquist, 1997). A recent crystal structure of the complex between the chemotaxis phosphatase CheZ and response regulator CheY revealed similar intermolecular interactions (Zhao et al., 2002).

His-Asp Phosphotransfer in Two-Component Signaling Systems

The active sites of response regulators are well conserved and are composed of three carboxylate-containing residues and a lysine residue involved in coordinating an essential magnesium ion (reviewed in Stock et al., 2000; West and Stock, 2001). The arrangement of the side chains at the active site of SLN1-R1 closely resembles that of the unphosphorylated response regulator CheY without the active site magnesium ion (Volz and Matsumura, 1991) (PDB code: 3CHY). The conserved residues in the active site of SLN1-R1 (Glu1094, Asp1095, Asp1144, and Lys1195) are positioned similarly as the corresponding residues in CheY (Asp12, Asp13, Asp57, and Lys109). Despite being crystallized in the presence of $MgCl_2$ and a phosphate analog (beryllium fluoride) (Chooback and West, 2003), no visible electron density for the metal ion or BeF_3^- was observed in the active sites of SLN1-R1 in either crystal form. However, the inclusion of beryllium fluoride in the crystallization conditions favored formation of the orthorhombic crystals (Chooback and West, 2003). Previous

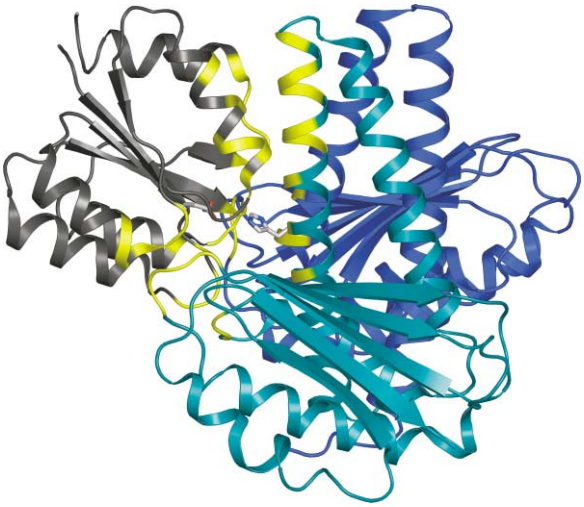

Figure 5. A Ribbon Representation of the Spo0F-Spo0B Complex

The response regulator Spo0F (gray) forms contacts to both the four helix bundle and flanking α/β domain of the homodimeric Spo0B protein (each monomer is shown in a different shade of blue) (PDB code: 1F51). Regions of the Spo0F that are involved in forming contacts to Spo0B are highlighted in gold (Zapf et al., 2000). The active site residues, His30 and Asp54, are shown in stick model. For simplicity, only one molecule of Spo0F is shown here.

studies with homologous response regulators indicated that the side chain orientation of two additional residues located near the active site (Thr87 and Tyr106 in CheY) is correlated to the phosphorylation state of response regulators (Birck et al., 1999; Cho et al., 2000; Halkides et al., 2000; Kern et al., 1999; Lee et al., 2001; Lewis et al., 1999). The side chain conformations of the corresponding residues in SLN1-R1 (Thr1173 and Phe1192) indicate that the SLN1-R1 structures determined in this study represent the unphosphorylated state of the response regulator.

Overall, there is very low sequence homology among HPt proteins except in the region near the histidine phosphorylation site (Xu and West, 1999). The structures of HPt proteins that have been determined, however, reveal much greater structural homology. All HPt proteins feature a solvent-exposed histidine phosphorylation site at similar locations on the surface of a four helix bundle. The two antiparallel helices facing the same side as the histidine show the greatest structural similarity, with the helical hairpins in YPD1, ArcB^c, and the CheA P1 domain superimposing very well with each other (Figures 4A and 4B). More specifically, the positioning of the histidine phosphorylation site on the helix surface and its side chain conformation (χ_1 ~178.5° and χ_2 ~72.8°) is well conserved. The conserved shape of the HPt surface around its phosphorylation site provides easy access of the histidine to the active site of the response regulators.

In both the $P2_12_12_1$ model and the $P3_2$ model of the YPD1/SLN1-R1 complex, His64 is in close proximity to the active site of SLN1-R1. However, in the $P2_12_12_1$ complex, His64 from YPD1 is much closer to the active site of SLN1-R1. In addition, a sulfate ion (presumably from the crystallization solution) is located near the Nδ1 atom of His64 and is involved in forming a network of H bond interactions, specifically to His64, Lys67, and Gln86 from YPD1, and Ala1174, Lys1195, and Thr1173 from SLN1-R1 (Figure 6A). Although not in a position to mimic a phosphoryl group, the presence of this sulfate ion, influences the side chain conformations of His64, Lys67, and Gln86 in YPD1, which all differ slightly from the YPD1 structure determined alone (Xu and West, 1999). Furthermore, the side chain position for His64 from YPD1 in the complex is affected by an additional H bond interaction between the Nϵ2 atom of His64 and Asp1095 from SLN1-R1. Consequently, the His64 side chain is shifted into an area normally occupied by a magnesium ion, and the side chain conformation is different than that observed in the YPD1 structure determined alone (Xu and West, 1999) (Figure 6B). The alignment and distance (4.58 Å) between Nϵ2 of His64 from YPD1 and Oδ1 of Asp1144 from SLN1-R1 in the $P2_12_12_1$ complex is not ideal for phosphoryl transfer to occur. However, a magnesium ion can easily be modeled into the active site at a position similar to other response regulators (Lewis et al., 1999; Stock et al., 1993) with reasonable geometry and distances without the need to change the structure of SLN1-R1. With the His64 side chain moved back to its original side chain conformation (as in the YPD1 structure alone), the Nϵ2 atom of His64 is better aligned for phosphotransfer to occur based on the active site configuration in the $P2_12_12_1$ complex (Figure 6B). The distance between Nϵ2 of His64 and Oδ1 of Asp1144 is then 4.8 Å, which is consistent with what is observed in the Spo0B/Spo0F complex (Zapf et al., 2000). Based on the analysis of the active site of the $P2_12_12_1$ complex, the transition state representative of a His-Asp phosphotransfer reaction can easily be realized without major structural changes to either YPD1 or SLN1-R1 (Figure 6B). Therefore, we propose that the $P2_12_12_1$ crystal structure of the YPD1/SLN1-R1 complex is representative of a productive complex.

Specificity of HPt Protein/Response Regulator Protein Interactions

YPD1 can interact with several different response regulators, including bacterial CheY (Janiak-Spens et al., 1999). This apparent lack of specificity of YPD1 toward response regulator domains is understandable in that YPD1 has evolved to bind to more than one response regulator in vivo. The binding surface of YPD1 is consistent with this property. Sequence alignment and homology modeling suggests that SSK1-R2 and SLN1-R1 share similar hydrophobic surfaces near the α1 helix (our unpublished data). It seems likely that YPD1 interacts with response regulators through its conserved hydrophobic patch. As a result, YPD1 may have evolved to function as a generic type of HPt domain that can interact with several different but homologous response regulator domains.

Previous studies have shown that YPD1 binds to the response regulator domain from SSK1 preferentially, and a complex was detectable by a native gel shift assay but only when the response regulator was phosphorylated (Janiak-Spens et al., 2000). Thus, binding affinity can be affected by several factors including the phosphorylation state of either protein. For example, surface complementarity between YPD1 and each response regulator domain may differ, and consequently, the size

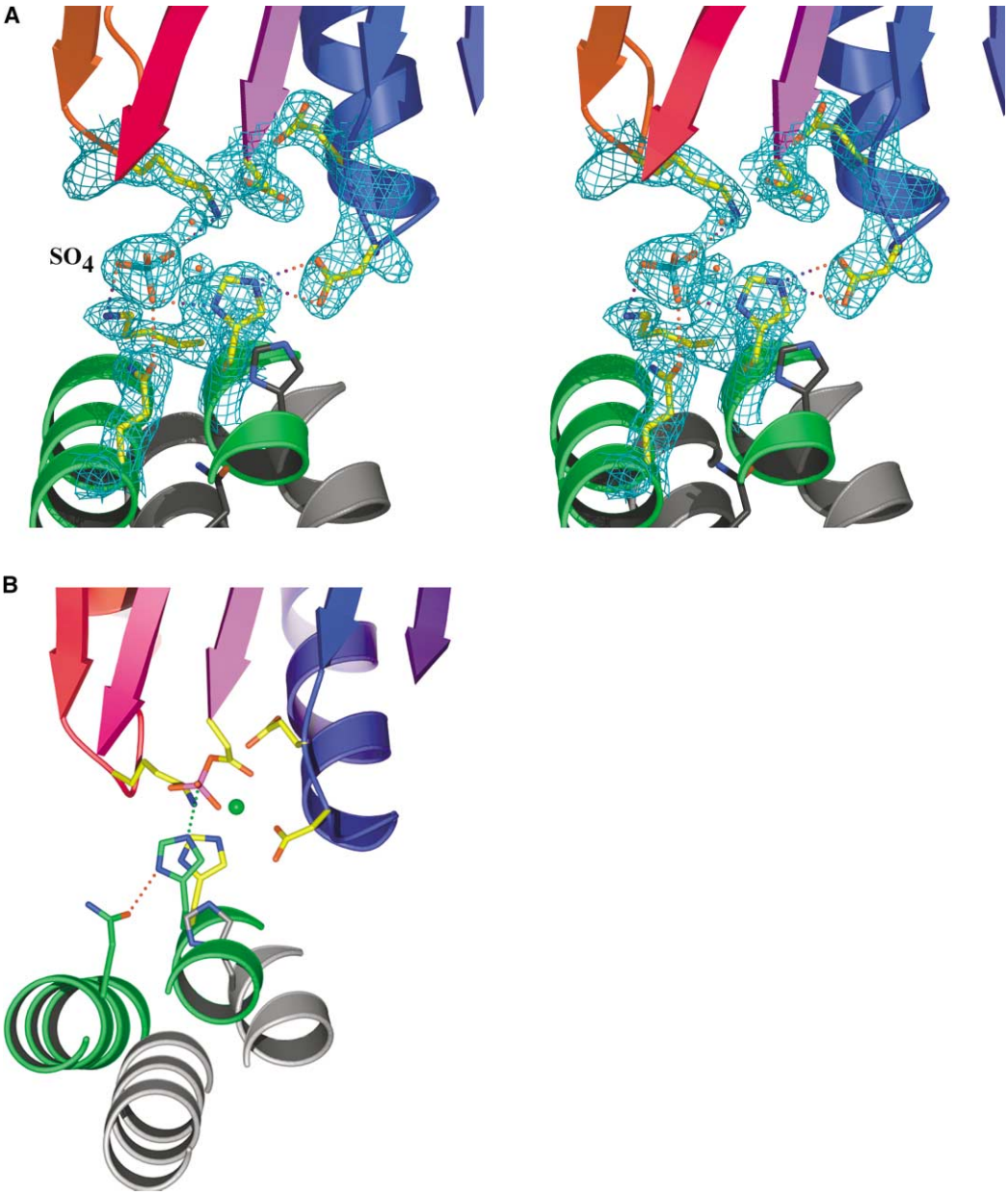

Figure 6. Active Site Configuration and His-Asp Transfer Mechanism

(A) Stereoview of the electron density ($2F_o$-F_c map contoured at 1.5 σ) at the active site of the $P2_12_12_1$ form of the YPD1/SLN1-R1 complex. The structure of the $P3_2$ form was overlaid onto the $P2_12_12_1$ form by superimposing the SLN1-R1 domains. The displaced location of helices αC and αD and His64 and Gln86 in the $P3_2$ complex are shown in gray, and also illustrates the conformational differences between the two models. Density for the sulfate ion is also shown and hydrogen bond interactions are indicated by the dotted lines.

(B) A transition state model based on the $P2_12_12_1$ model of the YPD1/SLN1-R1 complex. By slightly changing the conformation of His64 side chain from what is observed in the YPD1/SLN1-R1 crystal structures (yellow bonds) to a conserved conformation (green bonds) as seen in the crystal structure of YPD1 alone (PDB code: 1QSP), the Nϵ2 atom is properly aligned for phosphotransfer as modeled in the active site of SLN1-R1. A modeled phosphoryl group is shown in red stick model bonded to Asp1144 of the SLN1-R1 domain. An essential magnesium ion (green sphere) can also be modeled into a similar location at the active site of SLN1-R1 based on analysis of coordination geometry of other homologous response regulator structures complexed with metal ions (PDB codes: 1QMP, 2CHE).

of the buried hydrophobic binding site may also vary. In addition, a significant portion of the interactions at the interface is hydrophilic. As a result, hydrogen bonding or salt bridges may serve an important role in modulating intermolecular interactions. Further studies are necessary to determine which residues allow YPD1 to discriminate between response regulator domains.

Experimental Procedures

Sample Preparation and X-Ray Data Collection

The *S. cerevisiae* YPD1 (full-length) and SLN-R1 (residues 1084–1220) proteins were overexpressed in *Escherichia coli*, purified to homogeneity, and cocrystallized as described (Chooback and West, 2003). Two crystal forms (Table 1) were obtained using 2.6 M ammonium sulfate as a precipitant under hanging drop vapor diffusion

conditions. X-ray diffraction data were collected at 100 K using a Rigaku/MSC RUH3R generator, R-Axis IV^{2+} image plate detector system, and Oxford Series 700 cryosystem. The data were processed using the HKL suite (Otwinowski and Minor, 1997) or D*TREK (Pflugrath, 1999). Data collection statistics are summarized in Table 1.

Molecular Replacement and Structure Refinement

The structure of the YPD1/SLN1-R1 complex in the $P3_2$ space group was solved by molecular replacement using the 2.7 Å structure of YPD1 (Xu and West, 1999) (PDB code: 1QSP) as the search template. The self-rotation search revealed a 2-fold noncrystallographic symmetry, and a cross-rotation calculation identified two significant peaks. However, cell content analysis based on a calculated Matthews' constant (Matthews, 1968) suggested that there were more than two molecules in the asymmetric unit. Searches with a single YPD1 model failed to separate signal from noise. A new search method, as implemented in the program MOLREP (Vagin and Teplyakov, 1997) of the CCP4 suite, which places two independently oriented YPD1 molecules simultaneously was used to determine the locations of the YPD1 molecules. By restricting the rotations of YPD1 to the two significant peaks found by the cross-rotation calculation, three pairs of YPD1 molecules were placed inside the unit cell giving a correlation coefficient (CC) of 0.389 and an R factor of 0.511 in space group $P3_2$ (CC = 0.347, R factor = 0.526 in $P3_1$) for resolution up to 3.0 Å. After rigid body refinement, the R factor dropped to 0.442 (R_{free} = 0.443) with starting R factor of 0.480 (R_{free} = 0.477) for all reflections to 2.1 Å (with bulk solvent correction).

Molecular replacement with a homologous response regulator domain (such as CheY) as a search probe was not successful. At this stage, there was no definitive electron density for identifying SLN1-R1. In order to improve the electron density for locating the SLN1-R1 domain, the initial phases calculated from six copies of YPD1 were improved using density modification techniques implemented in DM (Cowtan, 1994). Six-fold molecular averaging with noncrystallographic operators derived from YPD1 molecules dramatically improved the electron density of the regions in which SLN1-R1 was located and allowed for tracing of 75% of the backbone of the SLN1-R1 domain unambiguously. The backbone of CheY (Volz and Matsumura, 1991) (3CHY) was then overlaid onto the above trace with rms deviation of ~1.0 Å and served as a reference for tracing the rest of the SLN1-R1 structure. After several rounds of density modification and model rebuilding, an initial model of SLN1-R1 containing 97 residues (674 atoms) was obtained and used for subsequent refinement and model rebuilding. The rest of the SLN1-R1 molecules in the asymmetric unit were generated by the noncrystallographic operators derived from the YPD1 molecules. Each of the six YPD1/SLN1-R1 complexes was constrained to be identical for the early stages of refinement by program CNS (Brünger et al., 1998). The initial R factor dropped from 0.408 (R_{free} = 0.408) to 0.330 (R_{free} = 0.332) after one cycle of rigid body refinement, simulated annealing refinement of torsion angle, and B factor refinement. After several cycles of refinement and model rebuilding, the R factor improved to 0.301 (R_{free} = 0.302). The constraints between complexes related by noncrystallographic symmetry were then replaced by strict restraints and models were further refined using the program REFMAC (Murshudov et al., 1997) and rebuilt in XtalView (McRee, 1999). The final model contains six copies of YPD1/SLN1 complexes with 1704 residues and 225 solvent molecules (18 SO_4^{2-} and 207 H_2O molecules) and demonstrates good geometry. Backbone dihedral angles for all nonglycine residues except Lys1149 fall into allowable regions of a Ramachandran plot with 94.1% of the residues in the most favored area as defined in program PROCHECK (Laskowski et al., 1993). The backbone dihedral angles of the residue Lys1149 in SLN1-R1 is conserved in response regulator domains such as CheY but falls into the disallowed area. Several areas in both proteins were not modeled due to poor electron density; these correspond to residues 22–25 and 126–131 in YPD1 and 1084–1086 (N terminus) and 1215–1220 (C terminus) in SLN1-R1. The final crystallographic R factor for the $P3_2$ model is 0.236 (R_{free} = 0.258).

The complex structure between YPD1 and SLN1-R1 in space group $P2_12_12_1$ was determined by molecular replacement using independent models of SLN1-R1 and YPD1 as obtained in the $P3_2$ space group. There is one YPD1/SLN1-R1 complex per asymmetric unit corresponding to ~54% solvent content (compared to ~46% in space group $P3_2$). The final R factor for the refined model was 0.214 (R_{free} = 0.266). The final refinement statistics for both complexes are summarized in Table 1.

Molecular Modeling of CheA-P1 Domain and CheY Interaction

Since YPD1 and the CheA-P1 domain are highly related, the complex of YPD1/SLN1-R1 provides a good general model for studying CheA-P1 domain and CheY interactions as well. The theoretical model of a CheY, CheA-P1 domain, and CheA-P2 domain ternary complex was constructed using the YPD1/SLN1-R1 complex ($P2_12_12_1$) and the CheY/CheA-P2 complex (Welch et al., 1998) (PDB code: 1A0O) as templates. First, the homologous response regulator domains in the two complexes, i.e., SLN1-R1 and CheY (Stock et al., 1993) (PDB code: 2CHE), were overlaid onto each other. Then the CheA-P1 domain (Mourey et al., 2001) (PDB code: 1I5N) was overlaid onto YPD1 by structural superimposition. The CheA-P1 domain and the CheA-P2/CheY complex in the above orientations were then combined to produce a model of the CheA-P1/CheY/CheA-P2 ternary complex.

Molecular Graphics

The figures in this paper were prepared using PYMOL (DeLano, 2002) or MOLSCRIPT (Kraulis, 1991) combined with either RASTER3D (Merritt and Bacon, 1997) or GL_RENDER (http://www.hhmi.swmed.edu/external/Doc/Gl_render/Html/gl_render.html) unless specified otherwise.

Acknowledgments

We thank E. Enwall for assistance during data collection and F. Janiak-Spens for helpful discussions and critical reading of the manuscript. This work was supported by grants from the Oklahoma Center for the Advancement of Science and Technology and the National Institutes of Health. A.H.W. is a Cottrell Scholar of Research Corporation.

Received: June 5, 2003
Revised: August 19, 2003
Accepted: August 19, 2003
Published: December 2, 2003

References

Baikalov, I., Schröder, I., Kaczor-Grzeskowiak, M., Grzeskowiak, K., Gunsalus, R.P., and Dickerson, R.E. (1996). Structure of the *Escherichia coli* response regulator NarL. Biochemistry *35*, 11053–11061.

Birck, C., Mourey, L., Gouet, P., Fabry, B., Schumacher, J., Rousseau, P., Kahn, D., and Samama, J.-P. (1999). Conformational changes induced by phosphorylation of the FixJ receiver domain. Structure *7*, 1505–1515.

Brown, J.L., Bussey, H., and Stewart, R.C. (1994). Yeast Skn7p functions in a eukaryotic two-component regulatory pathway. EMBO J. *13*, 5186–5194.

Brünger, A.T., Adams, P.D., Clore, G.M., DeLano, W.L., Gros, P., Gross-Kunstleve, R.W., Jiang, J.-S., Kuzewski, J., Nilges, M., Pannu, N.S., et al. (1998). Crystallography and NMR system (CNS): a new software suite for macromolecular structure determination. Acta Crystallogr. D Biol. Crystallogr. *54*, 905–921.

Cho, H.S., Lee, S.-Y., Yan, D., Pan, X., Parkinson, J.S., Kustu, S., Wemmer, D.E., and Pelton, J.G. (2000). NMR structure of activated CheY. J. Mol. Biol. *297*, 543–551.

Chooback, L., and West, A.H. (2003). Co-crystallization of the yeast phosphorelay protein YPD1 with the SLN1 response regulator domain and preliminary X-ray diffraction analysis. Acta Crystallogr. D Biol. Crystallogr., *59*, 927–929.

Cowtan, K.D. (1994). "DM": an automated procedure for phase improvement by density modification. Joint CCP4 and ESF-EACBM Newsletter on Protein Crystallography *31*, 34–38.

DeLano, W.L. (2002). The PyMOL molecular graphics system (San Carlos, CA: DeLano Scientific).

Djordjevic, S., Goudreau, P.N., Xu, Q., Stock, A.M., and West, A.H. (1998). Structural basis for methylesterase CheB regulation by a phosphorylation-activated domain. Proc. Natl. Acad. Sci. USA *95*, 1381–1386.

Halkides, C.J., McEvoy, M.M., Casper, E., Matsumura, P., Volz, K., and Dahlquist, F.W. (2000). The 1.9 Å resolution crystal structure of phosphono-CheY, an analogue of the active form of the response regulator, CheY. Biochemistry *39*, 5280–5286.

Hoch, J.A., and Silhavy, T.J. eds. (1995). Two-Component Signal Transduction (Washington, DC: American Society for Microbiology Press).

Hoch, J.A., and Varughese, K.I. (2001). Keeping signals straight in phosphorelay signal transduction. J. Bacteriol. *183*, 4941–4949.

Hutchinson, E.G., and Thornton, J.M. (1996). PROMOTIF—a program to identify and analyze structural motifs in proteins. Protein Sci. *5*, 212–220.

Janiak-Spens, F., Sparling, D.P., and West, A.H. (2000). Novel role for an HPt domain in stabilizing the phosphorylated state of a response regulator domain. J. Bacteriol. *182*, 6673–6678.

Janiak-Spens, F., Sparling, J.M., Gurfinkel, M., and West, A.H. (1999). Differential stabilities of phosphorylated response regulator domains reflect functional roles of the yeast osmoregulatory SLN1 and SSK1 proteins. J. Bacteriol. *181*, 411–417.

Jones, S., Marin, A., and Thornton, J.M. (2000). Protein domain interfaces: characterization and comparison with oligomeric protein interfaces. Protein Eng. *13*, 77–82.

Kato, M., Mizuno, T., Shimizu, T., and Hakoshima, T. (1997). Insights into multistep phosphorelay from the crystal structure of the C-terminal HPt domain of ArcB. Cell *88*, 717–723.

Kern, D., Volkman, B.F., Luginbühl, P., Nohaile, M.J., Kustu, S., and Wemmer, D.E. (1999). Structure of a transiently phosphorylated switch in bacterial signal transduction. Nature *402*, 894–898.

Ketela, T., Brown, J.L., Stewart, R.C., and Bussey, H. (1998). Yeast Skn7p activity is modulated by the Sln1p-Ypd1p osmosensor and contributes to regulation of the HOG1 pathway. Mol. Gen. Genet. *259*, 372–378.

Kraulis, P.J. (1991). MOLSCRIPT: a program to produce both detailed and schematic plots of protein structures. J. Appl. Crystallogr. *24*, 946–950.

Laskowski, R.A. (1991). SURFNET: a program for visualizing molecular surfaces, cavities, and intermolecular interactions. J. Mol. Graph. *13*, 323–330.

Laskowski, R.A., MacArthur, M.W., Moss, D.S., and Thornton, J.M. (1993). PROCHECK: a program to check the stereochemical quality of protein structures. J. Appl. Crystallogr. *26*, 283–291.

Lee, S.-Y., Cho, H.S., Pelton, J.G., Yan, D., Henderson, R.K., King, D.S., Huang, L.-S., Kustu, S., Berry, E.A., and Wemmer, D.E. (2001). Crystal structure of an activated response regulator bound to its target. Nat. Struct. Biol. *8*, 52–56.

Lewis, R.J., Brannigan, J.A., Muchova, K., Barak, I., and Wilkinson, A.J. (1999). Phosphorylated aspartate in the structure of a response regulator protein. J. Mol. Biol. *294*, 9–15.

Li, S., Ault, A., Malone, C.L., Raitt, D., Dean, S., Johnston, L.H., Deschenes, R.J., and Fassler, J.S. (1998). The yeast histidine protein kinase, Sln1p, mediates phosphotransfer to two response regulators, Ssk1p and Skn7p. EMBO J. *17*, 6952–6962.

Madhusudan, Zapf, J., Whiteley, J.M., Hoch, J.A., Xuong, N.H., and Varughese, K.I. (1996). Crystal structure of a phosphatase-resistant mutant of sporulation response regulator Spo0F from *Bacillus subtilis*. Structure *4*, 679–690.

Matthews, B.W. (1968). Solvent content of protein crystals. J. Mol. Biol. *33*, 491–497.

McEvoy, M.M., Hausrath, A.C., Randolph, G.B., Remington, S.J., and Dahlquist, F.W. (1998). Two binding modes reveal flexibility in kinase/response regulator interactions in the bacterial chemotaxis pathway. Proc. Natl. Acad. Sci. USA *95*, 7333–7338.

McRee, D.E. (1999). Practical Protein Crystallography (San Diego, CA: Academic Press).

Merritt, E.A., and Bacon, D.J. (1997). Raster3D: photorealistic molecular graphics. Methods Enzymol. *277*, 505–524.

Mourey, L., Da Re, S., Pédelacq, J.-D., Tolstykh, T., Faurie, C., Guillet, V., Stock, J.B., and Samama, J.-P. (2001). Crystal structure of the CheA histidine phosphotransfer domain that mediates response regulator phosphorylation in bacterial chemotaxis. J. Biol. Chem. *276*, 31074–31082.

Müller-Dieckmann, H.-J., Grantz, A.A., and Kim, S.-H. (1999). The structure of the signal receiver domain of the *Arabidopsis thaliana* ethylene receptor ETR1. Structure *7*, 1547–1556.

Murshudov, G.N., Vagin, A.A., and Dodson, E.J. (1997). Refinement of macromolecular structures by the maximum-likelihood method. Acta Crystallogr. D Biol. Crystallogr. *53*, 240–255.

Nooren, I.M.A., and Thornton, J.M. (2003). Structural characterisation and functional significance of transient protein-protein interactions. J. Mol. Biol. *325*, 991–1018.

Otwinowski, Z., and Minor, W. (1997). Processing of X-ray diffraction data collected in oscillation mode. Methods Enzymol. *276*, 307–326.

Pflugrath, J.W. (1999). The finer things in X-ray diffraction data collection. Acta Crystallogr. D Biol. Crystallogr. *55*, 1718–1725.

Porter, S.W., Xu, Q., and West, A.H. (2003). Ssk1p response regulator binding surface on histidine-containing phosphotransfer protein Ypd1p. Eukaryot. Cell *2*, 27–33.

Posas, F., Wurgler-Murphy, S.M., Maeda, T., Witten, E.A., Thai, T.C., and Saito, H. (1996). Yeast HOG1 MAP kinase cascade is regulated by a multistep phosphorelay mechanism in the SLN1–YPD1-SSK1 "two-component" osmosensor. Cell *86*, 865–875.

Robinson, V.L., Buckler, D.R., and Stock, A.M. (2000). A tale of two components: a novel kinase and a regulatory switch. Nat. Struct. Biol. *7*, 626–633.

Saito, H. (2001). Histidine phosphorylation and two-component signaling in eukaryotic cells. Chem. Rev. *101*, 2497–2509.

Song, H.K., Lee, J.Y., Lee, M.G., Min, J.M.K., Yang, J.K., and Suh, S.W. (1999). Insights into eukaryotic multistep phosphorelay signal transduction revealed by the crystal structure of Ypd1p from *Saccharomyces cerevisiae*. J. Mol. Biol. *293*, 753–761.

Stock, A.M., Martinez-Hackert, E., Rasmussen, B.F., West, A.H., Stock, J.B., Ringe, D., and Petsko, G.A. (1993). Structure of the Mg^{2+}-bound form of CheY and mechanism of phosphoryl transfer in bacterial chemotaxis. Biochemistry *32*, 13375–13380.

Stock, A.M., Robinson, V.L., and Goudreau, P.N. (2000). Two-component signal transduction. Annu. Rev. Biochem. *69*, 183–215.

Tomomori, C., Tanaka, T., Dutta, R., Park, H., Saha, S.K., Zhu, Y., Ishima, R., Liu, D., Tong, K.I., Kurokawa, H., et al. (1999). Solution structure of the homodimeric core domain of *Escherichia coli* histidine kinase EnvZ. Nat. Struct. Biol. *6*, 729–734.

Urao, T., Yamaguchi-Shinozaki, K., and Shinozaki, K. (2000). Two-component systems in plant signal transduction. Trends Plant Sci. *5*, 67–74.

Vagin, A., and Teplyakov, A. (1997). MOLREP: an automated program for molecular replacement. J. Appl. Crystallogr. *30*, 1022–1025.

Varughese, K.I., Madhusudan, Zhou, X.Z., Whiteley, J.M., and Hoch, J.A. (1998). Formation of a novel four-helix bundle and molecular recognition sites by dimerization of a response regulator phosphotransferase. Mol. Cell *2*, 485–493.

Volkman, B.F., Nohaile, M.J., Amy, N.K., Kustu, S., and Wemmer, D.E. (1995). Three-dimensional solution structure of the N-terminal receiver domain of NTRC. Biochemistry *34*, 1413–1424.

Volz, K., and Matsumura, P. (1991). Crystal structure of *Escherichia coli* CheY refined at 1.7-Å resolution. J. Biol. Chem. *266*, 15511–15519.

Wallace, A.C., Laskowski, R.A., and Thornton, J.M. (1995). LIGPLOT: a program to generate schematic diagrams of protein-ligand interactions. Protein Eng. *8*, 127–134.

Welch, M., Chinardet, N., Mourey, L., Birck, C., and Samama, J.-P.

(1998). Structure of the CheY-binding domain of histidine kinase CheA in complex with CheY. Nat. Struct. Biol. *5*, 25–29.

West, A.H., and Stock, A.M. (2001). Histidine kinases and response regulator proteins in two-component signaling systems. Trends Biochem. Sci. *26*, 369–376.

Xu, Q., and West, A.H. (1999). Conservation of structure and function among histidine-containing phosphotransfer (HPt) domains as revealed by the crystal structure of YPD1. J. Mol. Biol. *292*, 1039–1050.

Zapf, J., Sen, U., Madhusudan, Hoch, J.A., and Varughese, K.I. (2000). A transient interaction between two phosphorelay proteins trapped in a crystal lattice reveals the mechanism of molecular recognition and phosphotransfer in signal transduction. Structure *8*, 851–862.

Zhao, R., Collins, E.J., Bourret, R.B., and Silversmith, R.E. (2002). Structure and catalytic mechanism of the *E. coli* chemotaxis phosphatase CheZ. Nat. Struct. Biol. *9*, 570–575.

Zhou, H., and Dahlquist, F.W. (1997). Phosphotransfer site of the chemotaxis-specific protein kinase CheA as revealed by NMR. Biochemistry *36*, 699–710.

Accession Numbers

Atomic coordinates have been deposited in the Protein Data Bank (accession code 1OXB for the $P2_12_12_1$ crystal complex and 1OXK for the $P3_2$ crystal complex).